The Meteoritical Society

Meteoritics & Planetary Science 1–16 (2019)
doi: 10.1111/maps.13375

Cr isotopes in physically separated components of the Allende CV3 and Murchison CM2 chondrites: Implications for isotopic heterogeneity in the solar nebula and parent body processes

Yogita KADLAG*, Harry BECKER, and Andreas HARBOTT

Institut für Geologische Wissenschaften, Freie Universität Berlin, Malteserstr. 74-100, 12249 Berlin, Germany
*Corresponding author. E-mail: yogita@zedat.fu-berlin.de

(Received 06 December 2018; revision accepted 21 July 2019)

Abstract–Chromium isotopic data of physically separated components (chondrules, CAIs, variably magnetic size fractions) of the carbonaceous chondrites Allende and Murchison and bulk rock data of Allende, Ivuna, and Orgueil are reported to evaluate the origin of isotopic heterogeneity in these meteorites. Allende components show ε^{53}Cr and ε^{54}Cr from -0.23 ± 0.07 to 0.37 ± 0.05 and from -0.43 ± 0.08 to 3.7 ± 0.1, respectively. In components of Murchison, ε^{53}Cr and ε^{54}Cr vary from -0.06 ± 0.08 to 0.5 ± 0.1 and from 0.7 ± 0.2 to 1.7 ± 0.1, respectively. The non-systematic variations of ε^{53}Cr and ^{55}Mn/^{52}Cr in the components of Allende and Murchison were likely caused by small-scale, alteration-related redistribution of Mn >20 Ma after formation of the solar system. Chondrule fractions show the lowest ^{55}Mn/^{52}Cr and ε^{54}Cr values of all components, consistent with evaporation of Mn and ε^{54}Cr-rich carrier phases from chondrule precursors. Components other than the chondrules show higher Mn/Cr and ε^{54}Cr, suggestive of chemical and isotopic complementarity between chondrules and matrix-rich fractions. Bulk rock compositions calculated based on weighted compositions of components agree with measured Cr isotope data of bulk rocks, in spite of the Cr isotopic heterogeneity reported by the present and previous studies. This indicates that on a sampling scale comprising several hundred milligrams, these meteorites sampled isotopically and chemically homogeneous nebular reservoirs. The linear correlation of ^{55}Mn/^{52}Cr with ε^{53}Cr in bulk rocks likely was caused by variable fractionation of Mn/Cr, subsequent mixing of phases in nebular domains, and radiogenic ingrowth of ^{53}Cr.

INTRODUCTION

The moderately volatile transition metal Cr has three stable isotopes, ^{52}Cr (83.789%), ^{53}Cr (9.501%), and ^{54}Cr (2.365%), and ^{50}Cr (4.345%) is a nearly stable isotope, which may decay to ^{50}Ti with a half-life $>1.8 \times 10^{17}$ years (Norman 1985). ^{50}Cr, ^{52}Cr, and ^{53}Cr can be produced in explosive silicon and oxygen burning in supernovae (Woosley et al. 2002). ^{53}Cr is also produced by the decay of ^{53}Mn with a half-life of 3.7 (±10%) Ma (Honda and Imamura 1971). In contrast, ^{54}Cr is produced in the neutron-rich ejecta from type Ia supernovae (Clayton 2003). Variations in the ^{53}Cr/^{52}Cr and ^{54}Cr/^{52}Cr ratios are observed in all chondrite classes in comparison to terrestrial materials (Lugmair and Shukolukov 1998; Shukolyukov and Lugmair 2004, 2006; Trinquier et al. 2007; Qin et al. 2010). Enstatite chondrites (EC) and ordinary chondrites (OC) show very similar ^{53}Cr/^{52}Cr ratios, which are slightly higher than the terrestrial standards (Trinquier et al. 2008b; Qin et al. 2010), but exhibit differences in their ^{54}Cr/^{52}Cr ratios (Trinquier et al. 2007; Qin et al. 2010). Carbonaceous chondrites (CC) yield large variations in ^{53}Cr/^{52}Cr and ^{54}Cr/^{52}Cr ratios and in general show enrichment of ^{53}Cr and ^{54}Cr in bulk rocks relative to the bulk silicate Earth (Trinquier et al. 2007). These observations suggest that there are variable endmembers with different Cr isotope ratios in chondrite classes and that there was a spatial and/or temporal heterogeneity in the distribution of the ^{54}Cr and ^{53}Cr carrier phases in the solar system.

The ^{54}Cr enrichment in CCs compared to terrestrial standards, EC, and OC can be attributed to the presence of different presolar components with heterogeneous Cr isotope compositions in the matrix of these meteorites (Zinner et al. 2005; Qin et al. 2009, 2011). The matrix abundance in different CC groups does not correlate with the ^{54}Cr anomaly of the chondrite bulk rocks (Qin et al. 2010). However, it was noted that the abundance of ^{54}Cr correlates with the degree of metamorphism of chondrite groups (Trinquier et al. 2007). These observations suggest that ^{54}Cr anomalies of CC matrices may have been diminished during metamorphic heating of chondrite parent bodies. However, these observations from the chondrite bulk rocks are in apparent conflict with the results from other chondrite components. Chondrules from petrologic type 3 CC chondrites (Vigarano and NWA 3118) show a much larger spread in their $^{54}Cr/^{52}Cr$ ratios compared to petrologic type 2 CC chondrites (NWA 6043, NWA 801, and LAP 02342; Olsen et al. 2016). The latter result contradicts the hypothesis that metamorphic heating homogenized Cr isotopes in chondrite parent bodies and diluted the high ^{54}Cr component. Thus, the origin of the ^{54}Cr isotopic heterogeneity and sources of anomalous Cr isotopes are still under investigation (Qin et al. 2009; Dauphas et al. 2010; Nittler et al. 2018).

Chondrules also possess variations in $^{53}Cr/^{52}Cr$, although error bars were large in previous work (Nyquist et al. 2001). Volatility-controlled elemental fractionation exists in chondrites for Mn and Cr, as most of the Mn is associated with matrix minerals (Lodders 2003), whereas Cr is found in more refractory components such as chondrules and in presolar grains in the matrices of CCs (Qin et al. 2009, 2010, 2011; Nittler et al. 2018). The $^{53}Cr/^{52}Cr$ isotopic heterogeneity in the inner solar system objects was interpreted in terms of radial heterogeneity of Mn/Cr caused by the different volatilities of Mn and Cr or by nonuniform mixing of newly injected nuclides from a nearby supernova explosion (Lugmair and Shukolukov 1998; Shukolyukov and Lugmair 2004, 2006). The value of the initial $^{53}Mn/^{55}Mn$ of the solar system is still debated (Birck and Allègre 1985, 1988; Lugmair and Shukolukov 1998; Nyquist et al. 2001, 2009; Shukolyukov and Lugmair 2006). More recent ^{53}Mn-^{53}Cr data have been interpreted to be consistent with a homogeneous initial $^{53}Mn/^{55}Mn$ of the solar system (Trinquier et al. 2008b; Yamashita et al. 2010). If this is correct, then ^{53}Mn-^{53}Cr can be used as a tool for dating fractionation processes in early solar system objects.

A better understanding of the Mn-Cr systematics and Cr isotope variations in CCs may also benefit from systematic determination of Cr-isotopic compositions of physically separated components such as CAIs, chondrules, matrix, and various size fractions. Significant variations of Cr isotope composition were reported from chondrules and refractory inclusions from CCs (Birck and Allègre 1988; Olsen et al. 2016). Effects from irradiation by cosmic rays on Cr isotopes may also occur and become more significant in samples with high Fe/Cr and higher exposure ages (Birck and Allègre 1988; Trinquier et al. 2008b; Qin et al. 2010). Consequently, the ^{54}Cr heterogeneity in different chondrite groups also may have a contribution from irradiated components with high Fe/Cr. Therefore, constraints on the cosmogenic effects can be obtained by the Cr isotopic analysis of the components with variable Fe/Cr.

Sequential dissolution of bulk samples of Orgueil (CI1), Tagish Lake (CI2), Sutter's Mill (CM2), and Murchison (CM2) (Trinquier et al. 2008b; Petitat et al. 2011; Yamakawa and Yin 2014) shows that large variations and differences exist in Cr-isotopic compositions of leachates and residues compared to the bulk rocks. The relative roles of mixing and grain-scale variations, parent body alteration, and incongruent leaching on chromium isotopic ratios in leaching experiments are sometimes unclear. The effects of chemical leaching in the laboratory in exposing isotopic variations may differ from natural hydrothermal processes or evaporation due to heating.

Complementarity of chemical and isotopic compositions (e.g., Mg/Si, W, and Mo nucleosynthetic isotope variations) was suggested for chondrules and matrix of CV and CM chondrites (Bland et al. 2005; Hezel and Palme 2008, 2010; Palme et al. 2015; Budde et al. 2016a, 2016b). In contrast, the existence of such a complementarity was challenged by a recent study of Mg and Cr isotope ratios in individual chondrules from CV chondrites (Olsen et al. 2016).

The purpose of the present study is threefold. First, systematic study of Cr isotope systematics in physically separated components of the CCs Allende (CV3) and Murchison (CM2) provides additional constraints on the issue of chondrule-matrix complementarity. Second, the variation of Cr isotope compositions with Fe/Cr in the components is used to constrain cosmogenic effects on the Cr isotope composition of CCs. Third, we aim to understand the origin and heterogeneity of radiogenic and nucleosynthetic Cr isotope variation in solar system objects.

METHOD AND SAMPLE PREPARATION

Sample Preparation

We have newly established the method of Cr separation and isotope analysis at Freie Universität Berlin, which is modified from Trinquier et al. (2008a) and Qin et al. (2010). In order to verify the accuracy of

results obtained by our method, we have also analyzed Cr isotope compositions of bulk rocks of the CCs Allende, Ivuna (both from the U.S. Museum of Natural History, Washington, D.C.), and Orgueil (Museum für Naturkunde, Berlin) along with a terrestrial Cr reference material (NIST 3112a Cr standard). Aliquots of 30–40 mg of homogeneous powders of bulk rock samples were dissolved in Savillex beakers, placed into Parr bombs using a 4:1 mixture of HF: HNO_3) (4 mL HF and 1 mL HNO_3) to obtain precise and accurate Cr isotope ratios of bulk rocks. A detailed description of the sample digestion procedure can be found in Wang et al. (2015).

For the analysis of separated components, nearly 1 g pieces of Allende (No.ME 2632, spec. no. 17, Field Museum, Chicago, IL) and Murchison (No.ME. 2684, spec. no. 23, Field Museum, Chicago, IL) were broken into fragments and different components such as chondrules and CAIs were separated from broken fragments. The remaining material was further separated into different grain size fractions (<20 μm, 20–80 μm, 80–150 μm, 150–200 μm, 200–250 μm, and >250 μm) using nylon sieves. The separated size fractions were further classified as magnetic, slightly magnetic, and nonmagnetic, depending on their magnetic behavior. Separated fractions were inspected under a binocular microscope and the photographs of separated components are included in the supporting information.

Samples used for acid digestion were weighed precisely and weights ranged from 2.2 to 61.9 mg. Samples were dissolved in reverse aqua-regia (1 mL HCl: 2 mL HNO_3) for 17 h at 320°C at 100 bar N_2 pressure in a high-pressure asher system (HPA-S). No residue was observed after acid digestion suggesting complete dissolution of samples. Digestion aliquots were analyzed for Re-Os systematics, highly siderophile elements (HSE: which includes Re, Os, Ir, Pt, Ru, Rh, Pd, and Au) abundances, chalcophile element (S, Se, and Te) abundances, major and minor element (Mg, Ca, Cr, Mn, Fe, Co, and Ni) abundances, and these data were reported elsewhere (Kadlag and Becker 2016). The remaining aliquots were split into two parts, one part was used to determine $^{55}Mn/^{52}Cr$ ratios and another part was used to determine precise Cr isotope compositions.

$^{55}Mn/^{52}Cr$ Ratios

$^{55}Mn/^{52}Cr$ ratios of the diluted digestion solutions were determined on an Element XR™ ICP-MS. Analyses were carried out in medium resolution mode with resolution power ≥4500 to eliminate possible doubly charged interferences on ^{52}Cr and ^{55}Mn from Pd^{++}, Ru^{++}, or Cd^{++}. A standard addition method was used to obtain precise ratios, taking into account the presence of matrix. Dissolved samples were diluted in 12 mL 0.28 M HNO_3 to obtain Cr concentrations in solutions of approximately 10 ppb. The diluted samples were split into four aliquots, 3 mL each. A mixed standard containing 10 ppm Cr and 5 ppm Mn was added to the three sample aliquots to obtain increasing concentrations of approximately 25, 50, and 75 ppb Cr and 12.5, 25, and 37.5 ppb Mn, respectively. Calibration curves were obtained for ^{52}Cr and ^{55}Mn mass fractions, and precise $^{55}Mn/^{52}Cr$ ratios were obtained for analyzed samples using linear regression. $^{55}Mn/^{52}Cr$ ratios of bulk rocks of the CCs, Ivuna, Orgueil, and Allende analyzed in this study (Table 1) are in good agreement with literature values (Rotaru et al. 1990; Shukolyukov and Lugmair 2006; Trinquier et al. 2008b; Qin et al. 2010). Typical uncertainties on $^{55}Mn/^{52}Cr$ ratios were <5% (2s) for most samples (Table 1).

Column Chemistry

For precise and interference-free analysis of Cr isotopes, Cr was separated from other elements using an effective and fast two-step column chromatography procedure, which was modified after Trinquier et al. (2008a) and Qin et al. (2010). In the first step, Fe is removed from the aliquot using 2 mL Eichrome anion exchange resin (AG1-X8 100-200 mesh) in polypropylene columns and 6 M HCl (Qin et al. 2010). The recovered Cr cut from the first separation step was dried down and dissolved in 1.5 M HCl. The second step of separation was carried out on glass columns using (2.4 mL) Bio-Rad cation exchange resin (AG50-X12 200-400). Chromium was eluted in 4.5 mL 1.5 M HCl and matrix elements such as Al, Ti, Na, Mg, V, and Mn were separated in later steps (15 mL 1.5 M HCl). Resin and columns were cleaned after separation using 6 M HCl. All collected cuts and cleaning acids were analyzed on the Element XR™ ICP-MS, to verify the efficiency of the separation and recovery of Cr on columns and blank contribution during the separation. The recovery of Cr in the first separation step was >99% for most samples and >97% for all samples in the second separation step. Because of the large quantity of Cr processed and analyzed, blank contributions (<0.4 ng) are negligible. The collected Cr cuts were dried down and treated with aqua-regia, followed by 14 M HNO_3 and 9 M HCl, respectively, several times and finally dissolved in 3–4 μL 6 M HCl for loading on filaments for isotope analysis.

Chromium Isotope Data Acquisition

Chromium isotopes were analyzed on a Thermo Finnigan Triton TIMS (thermal ionization mass spectrometer) in positive mode. About 1–2 μg of the purified Cr was mixed with H_3BO_3 and silica gel and

Table 1. $\varepsilon^{53}Cr$ and $\varepsilon^{54}Cr$ values, Mn/Cr and Fe/Cr ratios of separated components of Allende and Murchison, and bulk rock samples of Orgueil, Ivuna, and Allende analyzed in this study.

Meteorites	Samples	Weight (mg)	$\varepsilon^{53}Cr$	2σ	$\varepsilon^{54}Cr$	2σ	$^{55}Mn/^{52}Cr$	2σ	Fe/Cr	2σ
Allende	CAIs	3.4	0.04	0.07	3.72	0.06	1.90	0.20	129.7	40.3
	Chondrules	29	0.03	0.04	0.91	0.12	0.37	0.02	40.1	0.8
	Matrix (<20)	5.3	0.09	0.21	0.94	0.36	0.53	0.02	68.7	2.00
	Magnetic (20–80)	19	−0.04	0.16	0.70	0.24	0.55	0.07	70.0	1.1
	Magnetic (80–150)	50	0.36	0.07	1.30	0.12	0.53	0.01	71.2	1.0
	Magnetic (150–200)	13.7	0.04	0.05	0.84	0.04	0.53	0.06	68.4	1.6
	Magnetic (200–250)	27.8	0.28	0.14	1.23	0.16	0.54	0.08	75.5	1.3
	Slightly magnetic (20–80)	23.3	0.20	0.12	1.53	*0.23*	0.50	0.01	69.9	1.3
	Slightly magnetic (80–150)	61.9	−0.03	0.11	0.37	0.21	0.55	0.02	75.8	1.0
	Slightly magnetic (150–200)	22	0.23	0.05	1.10	0.08	0.55	0.09	74.5	1.5
	Slightly magnetic (200–250)	18.3	0.36	0.00	1.17	0.03	0.51	0.03	65.0	1.0
	Nonmagnetic	11.3	−0.24	0.09	−0.43	0.03	1.37	0.04	96.6	4.8
	Calculated bulk rock	600	0.19	0.08	0.97	0.21	0.55	0.05	67.1	1.2
Murchison	Chondrules	2.2	0.04	0.21	0.88	0.08	0.58	0.07	29.4	2.6
	Magnetic (20–80)	18.1	0.29	***0.10***	1.70	***0.17***	0.82	0.27	73.9	1.7
	Magnetic (80–150)	15	−0.07	***0.10***	1.46	***0.18***	0.72	0.04	79.8	1.5
	Magnetic (150–200)	16.6	0.34	***0.10***	1.36	***0.18***	1.22	0.25	120.6	2.5
	Magnetic (200–250)	2.3	0.15	***0.10***	1.16	***0.18***	0.83	0.13	75.7	4.6
	Magnetic (>250)	19.8	−0.27	0.04	0.86	0.49	0.92	0.05	94.1	1.5
	Slightly magnetic (20–80)	5.6	0.45	***0.15***	1.26	***0.26***	0.90	0.02	83.4	3.9
	Slightly magnetic (80–150)	24.1	0.35	***0.11***	1.06	0.04	0.79	0.05	73.2	1.3
	Slightly magnetic (150–200)	24.8	0.49	***0.16***	1.32	***0.27***	0.77	0.03	83.0	1.6
	Slightly magnetic (200–250)	5.1	0.13	0.25	0.94	0.11	1.17	0.14	94.5	6.0
	Slightly magnetic (>250)	17	0.18	0.16	1.17	0.05	0.87	0.05	84.8	1.5
	Nonmagnetic	41.8	0.10	***0.12***	0.66	***0.26***	0.74	0.03	40.7	1.0
	Nonmagnetic (20–80)	5.5	0.30	***0.11***	0.88	0.15	0.64	0.05	55.2	0.8
	Calculated bulk rock	650	0.09	0.13	1.10	0.18	0.84	0.12	81.1	1.5
Allende	Bulk rock	44.34	0.07	0.08	1.24	0.24	0.51	0.05		
Ivuna		30.47	0.30	0.17	1.79	0.20	0.94	0.05		
Orgueil		38.97	0.46	0.06	1.94	0.12	0.93	0.05		
Allende	Literature bulk rocks		0.10	0.09	0.90	0.12	0.46	0.05	64.1	10.0
Ivuna			0.42	0.01	1.53	0.17	0.82		74.2	13.4
Orgueil			0.31	0.24	1.58	0.20	0.86	0.11	69.8	10.0
Murchison			0.17	0.08	0.97	0.20	0.63	0.03	72.4	11.8

Reported uncertainties are SD or SE in case of more than two analyses (*n* is ranging from 2 to 6) of the same sample. Uncertainties reported by standard deviations are given in bold italics. Calculated bulk rock values are obtained from the mass balance of all components. Literature bulk rock data of Allende, Ivuna, Orgueil, and Murchison are the average values from different sources (Kallemeyn and Wasson 1981; Birck and Allègre 1988; Lodders 2003; Shukolyukov and Lugmair 2006; Moynier et al. 2007; Trinquier et al. 2008b; Qin et al. 2010; Petitat et al. 2011).

the mixture was loaded on W single filaments (Trinquier et al. [2008a] and Qin et al. [2010]). The filaments were heated to 1500 mA using an initial heating speed of 200 mA min^{-1}. The current was further increased up to 2000–2200 mA, using a speed of 50 mA min^{-1} or less, depending on the rate of increase in the intensity of the ^{52}Cr. The heating procedure was optimized to maintain a constant ion beam of 5–10 V on ^{52}Cr (10^{11} Ω resistor) during each analysis. All measurements were carried out in static collection mode. Potential interferences by ^{50}Ti, ^{50}V, and ^{54}Fe on ^{50}Cr and ^{54}Cr, respectively, were monitored by ^{49}Ti, ^{51}V, and ^{56}Fe. The following Faraday cup configuration was employed: L3 (^{49}Ti), L2 (^{50}[Ti + Cr + V]), L1 (^{51}V), C (^{52}Cr), H1 (^{53}Cr), H2 (^{54}[Cr + Fe]), and H3 (^{56}Fe). Intensities of the interfering elements were similar to background intensities for all samples, indicating successful separation of Cr from matrix elements, no efficient ionization of these elements occurred in the temperature range of Cr ionization, explaining the negligible interferences on the measured isotope ratios. NIST SRM 3112a Cr standard reference material (Lot No. 030730) was used as a terrestrial reference material. The $^{50}Cr/^{52}Cr$ ratio is corrected for instrument mass fractionation using $^{50}Cr/^{52}Cr = 0.051859$ (Shields et al. 1966) and applying the exponential mass fractionation law. Each measurement consisted of 28 blocks, with 20 cycles/block. Baseline was measured (30 cycles, counting

time = 1.05 s/cycle and prebaseline wait time = 10 s) and amplifier rotation was applied after every seventh block to eliminate cup biases. Most filaments were measured twice. Chromium isotopes of samples were normalized to NIST 3112a Cr standard and are expressed as ε^{i}Cr, where ε^{i}Cr is defined as $\varepsilon^{i}\mathrm{Cr} = ([^{i}\mathrm{Cr}/^{52}\mathrm{Cr}]_{\mathrm{sample}}/[^{i}\mathrm{Cr}/^{52}\mathrm{Cr}_{\mathrm{NIST\ 3112a}}]-1) \times 10^{4}$, where $i = 53$ or 54. The ε^{53}Cr and ε^{54}Cr values of samples are normalized with respect to the average values of $^{53}\mathrm{Cr}/^{52}\mathrm{Cr}_{\mathrm{NIST\ 3112a}}$ and $^{54}\mathrm{Cr}/^{52}\mathrm{Cr}_{\mathrm{NIST\ 3112a}}$ which were analyzed over the period of analysis. During this study (October 2014–January 2016, $n = 39$), the reproducibility on the Cr isotope measurements for Cr standard NIST 3112a was 0.05 (2SE) for ε^{53}Cr and 0.06 (2SE) for ε^{54}Cr. For each measurement session ($n = 2$), repeatability on the Cr isotope measurements for Cr standard NIST 3112a was 0.1 (2SE) for ε^{53}Cr and 0.1 (2SE) for ε^{54}Cr.

RESULTS

New data of $^{55}\mathrm{Mn}/^{52}\mathrm{Cr}$ ratios, ε^{53}Cr, and ε^{54}Cr on bulk rock samples of Allende, Ivuna, and Orgueil from this study and mean values from the literature are listed in Table 1. Bulk rock ε^{53}Cr values of Allende, Ivuna, and Orgueil are 0.07 ± 0.08, 0.30 ± 0.17, and 0.46 ± 0.06, respectively (uncertainties are 2SE, $n = 3$–5). Bulk rock ε^{54}Cr values of Allende, Ivuna, and Orgueil are: 1.24 ± 0.24, 1.79 ± 0.22, and 1.94 ± 0.12, respectively. $^{55}\mathrm{Mn}/^{52}\mathrm{Cr}$ ratios of bulk rocks of Allende, Ivuna, and Orgueil are 0.51 ± 0.05, 0.94 ± 0.05, and 0.93 ± 0.05 (2SD), respectively (Table 1).

Within uncertainties, the ε^{53}Cr, ε^{54}Cr, and $^{55}\mathrm{Mn}/^{52}\mathrm{Cr}$ values of the bulk rock samples of Allende, Ivuna, and Orgueil are in agreement with literature values (Table 1). The isotopic mass balance of components suggests that calculated bulk rock values ($\varepsilon^{53}\mathrm{Cr}_{\mathrm{calc\ Allende}} = 0.19 \pm 0.08$, $\varepsilon^{54}\mathrm{Cr}_{\mathrm{calc\ Allende}} = 0.97 \pm 0.21$, and $\mathrm{Mn/Cr}_{\mathrm{calc\ Allende}} = 0.55 \pm 0.05$; $\varepsilon^{53}\mathrm{Cr}_{\mathrm{calc\ Murchison}} = 0.09 \pm 0.13$, $\varepsilon^{54}\mathrm{Cr}_{\mathrm{calc\ Murchison}} = 1.10 \pm 0.18$, and $\mathrm{Mn/Cr}_{\mathrm{calc\ Murchison}} = 0.84 \pm 0.12$) are similar within uncertainty to the analyzed bulk rocks (Kallemeyn and Wasson 1981; Birck and Allègre 1988; Shukolyukov and Lugmair 2006; Moynier et al. 2007; Trinquier et al. 2008b; Qin et al. 2010) from the literature ($\varepsilon^{53}\mathrm{Cr}_{\mathrm{Allende}} = 0.13 \pm 0.04$, $\varepsilon^{54}\mathrm{Cr}_{\mathrm{Allende}} = 0.9 \pm 0.1$, and $\mathrm{Mn/Cr}_{\mathrm{Allende}} = 0.46 \pm 0.05$; $\varepsilon^{53}\mathrm{Cr}_{\mathrm{Murchison}} = 0.17 \pm 0.08$, $\varepsilon^{54}\mathrm{Cr}_{\mathrm{Murchison}} = 0.97 \pm 0.20$, and $\mathrm{Mn/Cr}_{\mathrm{Murchison}} = 0.64 \pm 0.09$) and from this study ($\varepsilon^{53}\mathrm{Cr}_{\mathrm{Allende}} = 0.07 \pm 0.08$, $\varepsilon^{54}\mathrm{Cr}_{\mathrm{Allende}} = 1.24 \pm 0.24$, and $\mathrm{Mn/Cr}_{\mathrm{Allende}} = 0.51 \pm 0.05$).

The average $^{55}\mathrm{Mn}/^{52}\mathrm{Cr}$ ratio of CI chondrites is 0.94 ± 0.02. This compares to average $^{55}\mathrm{Mn}/^{52}\mathrm{Cr}$ of Orgueil and Ivuna of 0.86 ± 0.10 and 0.89 ± 0.11, respectively (Kallemeyn and Wasson 1981; Birck and Allègre 1988; Shukolyukov and Lugmair 2006; Moynier et al. 2007; Trinquier et al. 2008b; Qin et al. 2010; Lodders 2003). $^{55}\mathrm{Mn}/^{52}\mathrm{Cr}$ ratios of components of Allende analyzed in this study vary from 0.37 ± 0.02 to 1.90 ± 0.20 (Table 1). In components of Murchison, $^{55}\mathrm{Mn}/^{52}\mathrm{Cr}$ ratios vary from 0.58 ± 0.07 to 1.22 ± 0.25. Hence, significant variations exist in components, compared to the bulk rocks. The chondrule fractions of both meteorites show the lowest $^{55}\mathrm{Mn}/^{52}\mathrm{Cr}$ ratio of the components (Table 1; Fig. 1).

The components of Allende show variations in ε^{53}Cr from -0.24 ± 0.09 to 0.36 ± 0.07 (2SE) and in ε^{54}Cr from -0.43 ± 0.03 to 3.72 ± 0.06 (2SE). The variation of ε^{53}Cr and ε^{54}Cr in the components of Murchison is from -0.27 ± 0.04 to 0.49 ± 0.16 (2SE) and from 0.66 ± 0.26 to 1.70 ± 0.17 (2SE), respectively. The nonmagnetic fraction of Allende shows the lowest ε^{53}Cr and ε^{54}Cr (Table 1; Fig. 2). The CAI fraction of Allende shows the highest ε^{54}Cr value, that is, 3.72 ± 0.06 (2SE). The magnetic, slightly magnetic, chondrule, and matrix fractions of both meteorites do not show linear variations between ε^{53}Cr and ε^{54}Cr, rather they mostly scatter around bulk rock values (Fig. 2). No systematic correlation is observed between

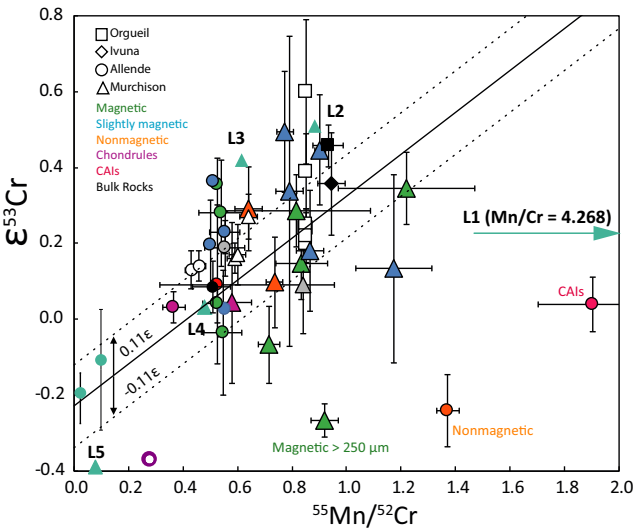

Fig. 1. Variation of ε^{53}Cr with Mn/Cr in the bulk rocks of Ivuna, Orgueil, Allende, and components of Allende and Murchison. White symbols are literature bulk rock data for Ivuna, Orgueil, Allende, and Murchison from various sources (Kallemeyn and Wasson 1981; Birck and Allègre 1988; Shukolyukov and Lugmair 2006; Moynier et al. 2007; Trinquier et al. 2008b; Qin et al. 2010; Petitat et al. 2011). Black solid correlation line is the bulk chondrite isochron from Trinquier et al. (2008b), who yield an initial ε^{53}Cr of -0.23 ± 0.11 and $^{53}\mathrm{Mn}/^{55}\mathrm{Mn} = (6.53 \pm 1.93) \times 10^{-6}$. Dashed lines reflect the uncertainties on $\varepsilon^{53}\mathrm{Cr}_{\mathrm{initial}}$. Leachate data of Murchison (L1–L5) and Allende (L1–L2) are from Yamakawa and Yin (2014) and Trinquier et al. (2008b).

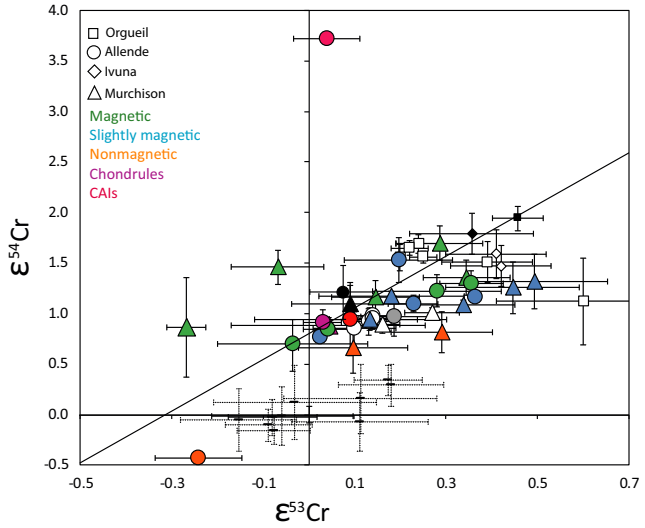

Fig. 2. $\varepsilon^{54}Cr$-$\varepsilon^{53}Cr$ variations in the bulk rocks of Ivuna (CI1), Orgueil (CI1), Allende (CV3), and components of Allende and Murchison (CM2). The CAI fraction from Allende shows the largest positive value of $\varepsilon^{54}Cr$ in this study. The lowest $\varepsilon^{54}Cr$ and $\varepsilon^{53}Cr$ are recorded in the refractory element enriched nonmagnetic fraction of Allende. All other components show a weak positive correlation between $\varepsilon^{54}Cr$ and $\varepsilon^{53}Cr$. Black and gray symbols are the bulk rock powder data (Allende, Ivuna, and Orgueil) and bulk rocks calculated from mass balance of all analyzed components, respectively. Dashed uncertainty bars show the 2SE (standard error) of multiple runs of the NIST Cr standard reference material during these measurements. White symbols are literature bulk rock data for Ivuna, Orgueil, Allende, and Murchison from various sources (Birck and Allègre 1988; Shukolyukov and Lugmair 2006; Moynier et al. 2007; Trinquier et al. 2008b; Qin et al. 2010; Petitat et al. 2011).

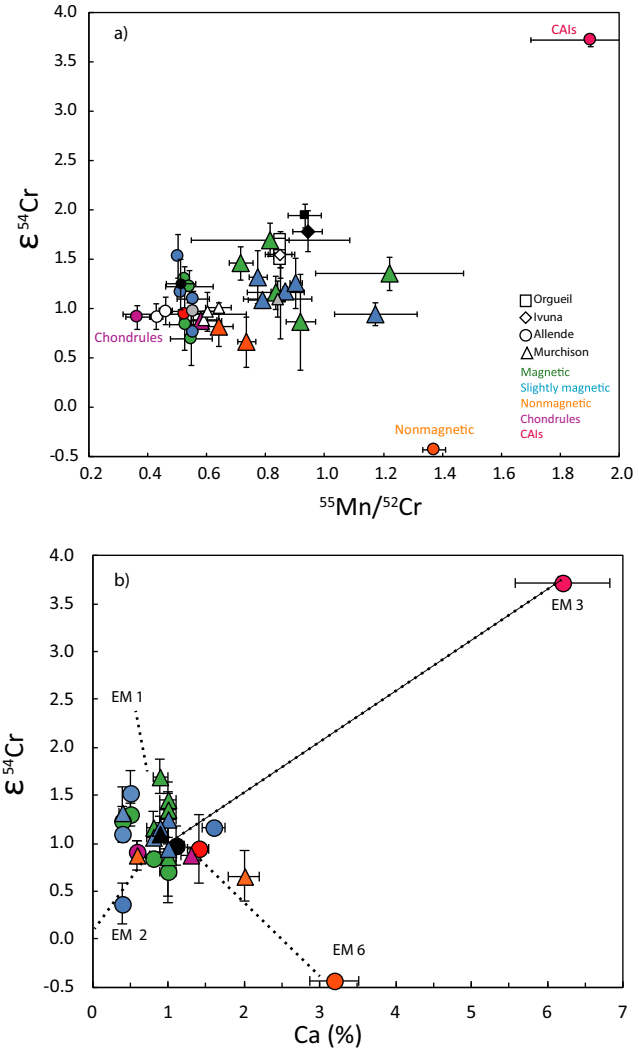

Fig. 3. a) Variation of $\varepsilon^{54}Cr$ with Mn/Cr in the bulk rocks of Ivuna, Orgueil, Allende, and components of Allende and Murchison. b) Variation of $\varepsilon^{54}Cr$ and Ca (wt%) in the components of Allende and Murchison. Calcium data from Kadlag and Becker (2016). Four endmember (EM) compositions of ^{54}Cr, which were defined in Yamakawa and Yin (2014) can be distinguished based on component data. The data suggest that the bulk rock compositions are mixtures of these endmembers. The legend is same as in Fig. 2.

$\varepsilon^{54}Cr$, $^{55}Mn/^{52}Cr$, Fe/Cr, Mg/Fe, Mn, and Cr concentrations (Figs. 2–4).

DISCUSSION

Measured and Calculated Cr Isotopic Composition of Bulk Chondrites

The agreement between measured bulk rock Cr isotope compositions of Allende, Orgueil, and Ivuna as well as the calculated bulk rock values of Allende and Murchison from the mass balance of all components with literature data is excellent (Table 1). This observation indicates that the Cr isotopic heterogeneity of components such as CAIs and presolar grains (the latter occur in slightly magnetic and nonmagnetic fractions of Allende), which show large variations at the component scale, is averaged out in bulk rocks at the scale of ≥1 g of sample. Our bulk rock data also show the linear correlation of $\varepsilon^{53}Cr$ with $^{55}Mn/^{52}Cr$ reported in the literature (Fig. 1). This correlation line is interpreted to reflect the presence of variable proportions of volatile-rich and -poor components in the different meteorites, which are representative of specific CC groups (Shukolyukov and Lugmair 2006; Trinquier et al. 2008b). Trinquier et al. (2008b) have shown that the correlation for bulk rocks from different groups of CCs yields $\varepsilon^{53}Cr_{initial} = -0.23 \pm 0.11$ and $^{53}Mn/^{55}Mn = (6.53 \pm 1.93) \times 10^{-6}$ with an age of this correlation of 4567.3 ± 1.9 Myr. The correction for

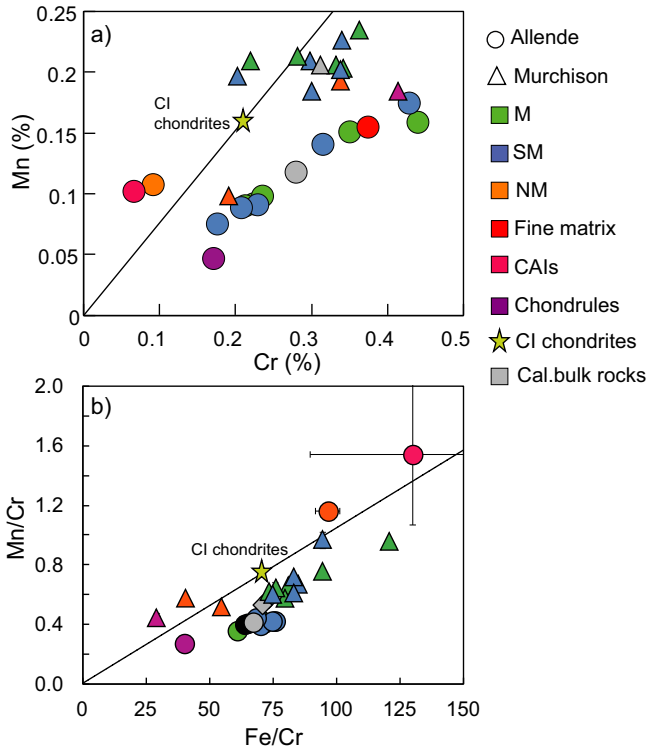

Fig. 4. a) Mn-Cr, (b) Mn/Cr-Fe/Cr variations in components of Allende and Murchison. CI chondrite data (Lodders 2003) is shown by the yellow star. Most components show deviation from the bulk rock value; however, the data define a linear correlation among Mn-Cr, Mn/Cr, and Fe/Cr suggesting that the deviation in Mn/Cr due to aqueous alteration is limited.

spallation produced Cr in the analyzed bulk rock powders and calculated bulk rocks from different components is negligible in CCs due to limited variation in Fe/Cr and the low cosmic ray exposure ages (Schultz and Franke [2004] and references therein). The present results suggest that despite the large variations observed in the components (Table 1; Fig. 2), an overall homogeneity of Cr isotope composition exists in the bulk rocks of Allende and Murchison for ≥1 g sample material.

Heterogeneity of ε^{53}Cr in Components of Allende and Murchison

Contrary to the bulk rocks, the components of Allende and Murchison show nonsystematic scatter of ε^{53}Cr and ^{55}Mn/^{52}Cr in the ^{53}Mn-^{53}Cr isochron diagram (Fig. 1). We note that most components such as chondrules; matrix; and some magnetic, slightly magnetic, and nonmagnetic fractions lie within uncertainties on the linear correlation between ε^{53}Cr and ^{55}Mn/^{52}Cr (Fig. 1) established from bulk chondrite data (Trinquier et al. 2008b). Two different endmember groups exist among the components: in the first group, components such as CAIs, the nonmagnetic fraction of Allende, and the >250 μm magnetic fraction of Murchison display significantly higher ^{55}Mn/^{52}Cr than the bulk rocks without correlated high ε^{53}Cr from radioactive decay of ^{53}Mn. In the second group (some magnetic and slightly magnetic components), variations in ε^{53}Cr occur at constant ^{55}Mn/^{52}Cr (Fig. 1). These observations suggest that either the ^{53}Mn-^{53}Cr systematics of components were disturbed on the parent bodies or in the solar nebula or that initial heterogeneity of ^{53}Mn existed in different components.

The random variations in the ^{53}Mn-^{53}Cr systematics of components of Allende and Murchison (Fig. 1) may reflect small-scale alteration on the parent bodies, which can produce significant deviations from the bulk CC isochron, if at the time of alteration ^{53}Mn/^{55}Mn ~0. The mobilization of Cr in olivine is evident in CCs of higher (>3.0) metamorphic grades (Grossman and Brearley 2005). From a recent study on diffusion kinetics of Cr and Mn in spinel, olivine, and orthopyroxene, we infer that parent body metamorphism should have affected Mn more than Cr (Posner et al. 2016). Therefore, metamorphic heating may have caused small-scale redistribution of Mn and Cr and the scatter of Allende components in the isochron diagram. Alteration effects are also evident from the variably disturbed Re-Os systematics of components of both Allende and Murchison analyzed in this study (Kadlag and Becker 2016). Secondary carbonate minerals such as dolomite in CM chondrites contain up to 5.7 wt% of Mn (Johnson and Prinz 1993; Riciputi et al. 1994; Fujiya et al. 2011). Previous studies have indicated that aqueous alteration on the Murchison parent body and formation of Mn-bearing calcites occurred during the lifetime of ^{53}Mn (Fujiya et al. 2012). Therefore, the difference of ε^{53}Cr between low-temperature minerals and high-temperature minerals of Murchison likely resulted from the redistribution of Mn during the formation of carbonate minerals and radiogenic ingrowth of ^{53}Cr.

The CAI fraction shows the highest ^{55}Mn/^{52}Cr (1.90) ratio compared to all components, but a lower ε^{53}Cr value than expected if ^{53}Mn was extant. Thus, the transport of Mn into the CAI fraction, which initially should have had a low Mn/Cr, likely occurred after most ^{53}Mn had decayed (i.e., >20 Ma after the formation of the solar system). The high porosity of fine-grained CAIs makes these plausible sites for precipitation of solutes from fluids during aqueous alteration and replacement of primary minerals by secondary alteration products (Brearley and Krot [2013] and references therein). Metamorphic heating may have

led to the transportation of hydrothermal fluids through the pores of fine-grained components of the Allende meteorite (Krot et al. 1995; Brearley and Krot 2013). Bland et al. (2009), considering the low permeability of chondrites, pointed out the difficulty of significant large-scale hydrothermal fluid flow. However, small-scale element redistribution between CAIs and matrix during localized aqueous alteration is likely and has affected Mn/Cr ratios of CAIs (Krot et al. 1995; Brearley and Krot 2013).

CAI fractions analyzed in this and previous studies (Papanastassiou 1986; Trinquier et al. 2008b) display variable ε^{53}Cr, ranging from –2.1 ± 1.1 to 0.04 ± 0.07. This might indicate that CAIs having higher ε^{53}Cr than the initial ε^{53}Cr of the solar system ($\varepsilon^{53}Cr_{SSinitial}$ ~ –0.23) show radiogenic ingrowth of ^{53}Cr from ^{53}Mn added early during alteration by volatile element-bearing gas in the nebula or during alteration by aqueous fluids during parent body metamorphism (Davis et al. 1994; Brearley et al. 2014). If we assume homogeneity of the ^{53}Mn distribution in the solar nebula at the time of formation of the CAIs, then the high Mn/Cr of the CAI fraction analyzed here requires 26% Mn to be either initially contained by the CAIs or added to CAIs within the lifetime of ^{53}Mn (likely in the solar nebula), while the rest of the Mn (74%) was added later to the CAIs after the decay of ^{53}Mn during thermal processing or late parent body alteration (>20 Ma after the formation of CAIs). It cannot be excluded that the CAIs had initial ^{53}Cr abundances different from other chondritic matter; however, such a scenario is not required to explain the data.

The major element, chalcophile, and HSE data of the nonmagnetic fraction from Allende suggest that it consists of refractory minerals (Kadlag and Becker 2016), yet its ^{55}Mn/^{52}Cr is also high and unsupported by its ε^{53}Cr value (Fig. 1). These data also indicate a role of late alteration in producing the high Mn/Cr, although this fraction shows no evidence for the disturbance of its Re-Os systematics by alteration processes (Kadlag and Becker 2016). Although the nonmagnetic fraction has a high ^{55}Mn/^{52}Cr ratio, the concentrations of Mn and Cr are low (Mn = 0.107 wt% and Cr = 0.092 wt%; Kadlag and Becker 2016) in this fraction. Thus, samples with anomalously high Mn/Cr (such as the CAI fraction and the nonmagnetic fraction) comprise only small fractions of the Mn and Cr (≤5% of total) in the bulk rocks and thus are insignificant for the bulk rock budget of these elements (Table 1). The nonmagnetic fraction of Allende also has the lowest ε^{53}Cr and ε^{54}Cr of all Allende components analyzed in the present work. The low ε^{53}Cr, which overlaps with the initial ε^{53}Cr of the solar system determined from the CC isochron, is not supported by the high Mn/Cr. Previous work suggests that negative ε^{53}Cr values are mainly associated with refractory minerals that show positive ε^{54}Cr (Trinquier et al. 2008b), which, surprisingly, is not observed in the nonmagnetic fraction of Allende. The depletion of ^{53}Cr in the latter fraction could reflect retarded ingrowth of ^{53}Cr, caused by originally low Mn/Cr in this component, prior to the presumed alteration processes that led to an increase of Mn/Cr in this fraction. This evolution is plausible because the nonmagnetic fraction is somewhat enriched in refractory elements such a Ca, Mg, and refractory HSEs (Kadlag and Becker 2016). However, in light of the negative ε^{54}Cr of this fraction, the existence of initial heterogeneity of ε^{53}Cr in some Allende components might be an alternative explanation (see below).

Heterogeneity of ε^{54}Cr in Components of Allende and Murchison

Variations of ε^{54}Cr in the components of Allende and Murchison are independent of the ^{55}Mn/^{52}Cr ratio, Fe/Cr ratio, and Mn and Cr concentrations (not shown here; see data in Kadlag and Becker 2016). Heterogeneity of ε^{54}Cr was also reported in sequential leachates of bulk rocks of Allende, Murchison, and several other CCs (Trinquier et al. 2008b; Petitat et al. 2011; Yamakawa and Yin 2014).

Trinquier et al. (2008b) observed variable positive deviations of ε^{54}Cr in different sequential leachates and CAI fractions of Allende, whereas a chondrule fraction showed slightly negative ε^{54}Cr = –0.08 ± 0.12. In another study, two individual Allende chondrules, C20 and C30, show ε^{54}Cr of –0.36 ± 0.09 and –0.58 ± 0.09, respectively (Connelly et al. 2012). With the exception of the nonmagnetic and CAI fractions of Allende, ε^{54}Cr of most Allende components in this study scatters between +0.6 and +1.6 (Fig. 2; Table 1), similar to leachates from previous work (Trinquier et al. 2008b). The CAI fraction of Allende shows a low Cr concentration (0.07 wt%), high ^{55}Mn/^{52}Cr ratio, and high positive ε^{54}Cr (Figs. 1–3), similar to previous data (Papanastassiou 1986; Birck and Lugmair 1988; Trinquier et al. 2008b; Mercer et al. 2015). In contrast, the nonmagnetic fraction of Allende, which is also enriched in refractory elements (Kadlag and Becker 2016), shows a low Cr concentration (0.092 wt%) and high ^{55}Mn/^{52}Cr ratio, but negative ε^{54}Cr of –0.43 ± 0.03. The latter observation is important as it implies the existence of refractory components in Allende with an origin and a history different from CAIs.

The very different ε^{54}Cr in these components result from carrier phases with a different history, origin, and

presumably different phase compositions. Because CAIs and the nonmagnetic fraction of Allende are enriched in refractory elements, the extreme endmember compositions in these materials may have been exposed to selective evaporation of presolar carrier grains at high temperatures (e.g., Trinquier et al. 2009) or carrier grains were added from different stellar sources at different times during the early evolution of the nebula (Yamakawa and Yin 2014; Schiller et al. 2015, 2018). As noted in the previous section, the nonmagnetic fraction from Allende also has a rather low $\varepsilon^{53}Cr$ of –0.24 ± 0.09, which overlaps the initial $\varepsilon^{53}Cr$ of the solar system (Trinquier et al. 2008b).

Values of $\varepsilon^{54}Cr$ in CAI fractions from Allende in previous studies range from –151.6 ± 4.2 to 48.5 ± 0.8 (Papanastassiou 1986; Birck and Lugmair 1988; Papanastassiou and Brigham 1989; Trinquier et al. 2008b; Mercer et al. 2015). The production of Cr isotopes due to cosmic ray-induced spallation reactions on Fe nuclides is an unlikely origin of these extreme variations, because production proportions are 0.2:1:1 for ^{50}Cr, ^{53}Cr, and ^{54}Cr, respectively (Shima and Honda 1966). In the case of the Allende CAI fraction in this study and in previous work (Papanastassiou 1986; Birck and Lugmair 1988; Papanastassiou and Brigham 1989; Trinquier et al. 2008b), deviations in $\varepsilon^{54}Cr$ are much larger than deviations in $\varepsilon^{53}Cr$ ($\varepsilon^{53}Cr$:$\varepsilon^{54}Cr$ of the CAI fraction is 1:96), ruling out major contributions from spallation-produced ^{54}Cr in Allende CAIs. Corrections for spallation-produced $\varepsilon^{54}Cr$ and $\varepsilon^{53}Cr$ in the CAI fraction from our work using the equation given in table 2 from Trinquier et al. (2007) are –0.001ε and –0.005ε, respectively, which is negligible. The enrichment of ^{54}Cr in the Allende CAI fractions was likely inherited from neutron-rich ejecta of type 1a supernovae during the neutron capture/beta-decay ($n\beta^-$) process and multizone mixing during nuclear statistical equilibrium (Hartmann et al. 1985). The enrichment of neutron-rich isotopes of Ti, Ni, and Zr in CAIs supports this scenario (Birck and Lugmair 1988; Leya et al. 2009; Mercer et al. 2015).

The variation of ^{54}Cr in the different CAI fractions analyzed in previous studies (Papanastassiou 1986; Birck and Lugmair 1988; Trinquier et al. 2008b; Mercer et al. 2015) shows a trimodal distribution (Fig. 5). The coarse-grained FUN inclusions analyzed by Papanastassiou (1986) show the lowest and highest $\varepsilon^{54}Cr$ in CAIs, that is, they plot on both sides of the main population of fine-grained CAIs, which show an average $\varepsilon^{54}Cr$ of 5.90 ± 1.95 (1σ). The CAI fraction analyzed in this study ($\varepsilon^{54}Cr$ = 3.72) apparently belongs to the main population (Fig. 5). The variable $\varepsilon^{54}Cr$ in the main CAI population of Allende is likely due to heterogeneous mixing of ^{54}Cr carriers.

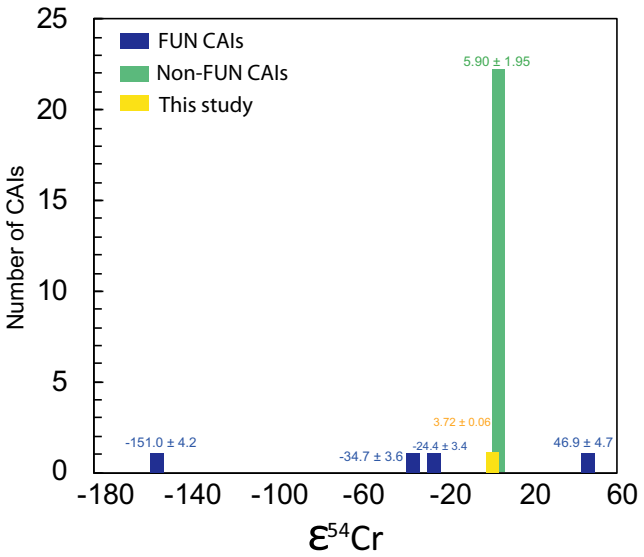

Fig. 5. Trimodal distribution of $\varepsilon^{54}Cr$ in the population of Allende CAIs analyzed so far (Papanastassiou 1986; Birck and Lugmair 1988; Papanastassiou and Brigham 1989; Bogdanovski et al. 2002; Trinquier et al. 2008a, 2008b; Mercer et al. 2015; this study). FUN-CAIs show the largest positive (46.9 ± 4.7) and negative (−151.0 ± 4.2) $\varepsilon^{54}Cr$ among physically separated components (Papanastassiou 1986; Papanastassiou and Brigham 1989). All non-FUN CAIs show enrichment and limited variation in $\varepsilon^{54}Cr$ relative to the standard reference material, which is likely due to initial heterogeneity in $\varepsilon^{54}Cr$ carriers followed by the variable thermal processing of CAIs in the protoplanetary disk (see Discussion).

Individual chondrules of Allende analyzed in previous studies show negative deviations in $\varepsilon^{54}Cr$, whereas the bulk chondrule population from this study shows $\varepsilon^{54}Cr$ similar to bulk rocks within uncertainty (Table 1). Heterogeneity also exists in matrix-rich fractions and other components; however, bulk rock Cr-isotopic compositions calculated from the components of Allende and Murchison are similar to the analyzed bulk rock data. These data indicate that although isotopic heterogeneity exists in components on the submillimeter scale, the majority of the grains or objects that define the components were formed from a reservoir of similar bulk isotopic composition. The complementary variation of ^{54}Cr in different components can be explained by stochastic sampling of isotopically heterogeneous grains from a reservoir with homogeneous bulk isotopic composition.

To conclude, $\varepsilon^{54}Cr$ heterogeneity exists in all components of Allende and Murchison, including CAIs, chondrules, and matrix separates. However, given that CC groups such as CV, CM, or CI chondrites have specific $\varepsilon^{54}Cr$ values, the larger variations observed in

components and in leachates must cancel at the bulk rock scale, as indicated by similar isotopic compositions of calculated and measured bulk rocks (this study). The heterogeneity of $\varepsilon^{54}Cr$ in the components is likely inherited from precursor material and at least partly results from variable thermal processing.

Comparison between Leachates and Physically Separated Components of Allende and Murchison

Previous studies of leachates and physically separated components show a heterogeneous distribution of s-process, r-process, and p-process isotopes in different leachate fractions of Murchison and Allende for many refractory elements such as Os, Ru, Ti, Cr, Sr, Zr, Mo, Ba, Nd, Sm, and W (Niemeyer 1988; Rotaru et al. 1992; Dauphas et al. 2002; Hidaka et al. 2003; Schönbächler et al. 2003, 2005; Trinquier et al. 2007, 2008b; Yokoyama et al. 2007; Reisberg et al. 2009; Burkhardt et al. 2012; Fischer-Gödde et al. 2015). The Cr isotope compositions of leachates of bulk rocks of Allende and Murchison displays large deviations of $^{54}Cr/^{52}Cr$ (Fig. 6) in different leachate fractions compared to bulk rocks and terrestrial Cr (Rotaru et al. 1992; Trinquier et al. 2008b; Yamakawa and Yin 2014). Two important observations emerge from the leachate studies. First, leachates of Murchison show large positive and negative anomalies ($\varepsilon^{54}Cr$ ranging from -15.49 ± 0.70 to 27.42 ± 0.70) compared to the NIST Cr standard reference material and the bulk rock of Murchison. In contrast, Allende leachates show rather limited variations in $\varepsilon^{54}Cr$ relative to the bulk rock (ranging from 2.54 ± 0.89 to -0.74 ± 0.70) relative to the NIST Cr standard.

Among physically separated components, CAIs, nonmagnetic fractions, and chondrule fractions show the largest deviation of $\varepsilon^{54}Cr$ in both positive and negative directions, respectively (this work; Papanastassiou 1986; Birck and Lugmair 1988; Papanastassiou and Brigham 1989; Trinquier et al. 2008b; Mercer et al. 2015). Second, the strongest enrichments in ^{54}Cr relative to the bulk rocks were observed in refractory element-rich (Murchison) and volatile element-rich (Allende) leachate fractions. The origin of the differences in Cr isotope composition of chemical leachates, physically separated components, and bulk rocks of both meteorites is not well understood. The different leachate studies on Murchison (Rotaru et al. 1992; Yamakawa and Yin 2014; Trinquier et al. 2007) suggest that similar leachate fractions recover isotopically heterogeneous Cr, for example, leachate L4 and L5 in Fig. 6, from different studies which show variable $\varepsilon^{54}Cr$ in the Murchison meteorite ($\varepsilon^{54}Cr$ in L4 is 15.44 ± 0.70, 16.12 ± 0.12, and 8.93 ± 0.08 and $\varepsilon^{54}Cr$ in L5 is 27.42 ± 0.70, 8.27 ± 0.12, and 15.74 ± 0.08). The heterogeneity of ^{54}Cr in similar leachates of Murchison may indicate either initial heterogeneity or variable dissolution of isotopically different Cr carrier phases during different stages of leaching. In the present study, we observe that $\varepsilon^{54}Cr$ in physically separated fractions is not as extreme as in leachate fractions of Murchison (e.g., $\varepsilon^{54}Cr$ in Murchison components ranges from 0.66 ± 0.26 to 1.70 ± 0.17 in this study). In contrast, in Allende, physically separated fractions show similar deviations as leachates. As outlined in the previous section, negative deviations in ^{54}Cr (and ^{53}Cr) are observed in the nonmagnetic, refractory element-enriched fraction of Allende, suggesting more than one presolar carrier phase of ^{54}Cr in these chondrites. The low abundances of ^{53}Cr and ^{54}Cr in the nonmagnetic fraction of Allende may reflect less ingrowth of ^{53}Cr in the Mn-poor refractory material with low abundances of ^{54}Cr.

Values of $\varepsilon^{53}Cr$ in leachates of Allende range from -0.12 ± 0.17 to 2.57 ± 0.07 and in chondrules and CAI fractions, the range is from -0.37 ± 0.07 to -1.64 ± 0.09, respectively (Rotaru et al. 1992; Trinquier et al. 2008b). $\varepsilon^{53}Cr$ in leachates of Murchison range from -0.76 ± 0.06 to 0.50 ± 0.06 (for comparison, physically separated components of Murchison show

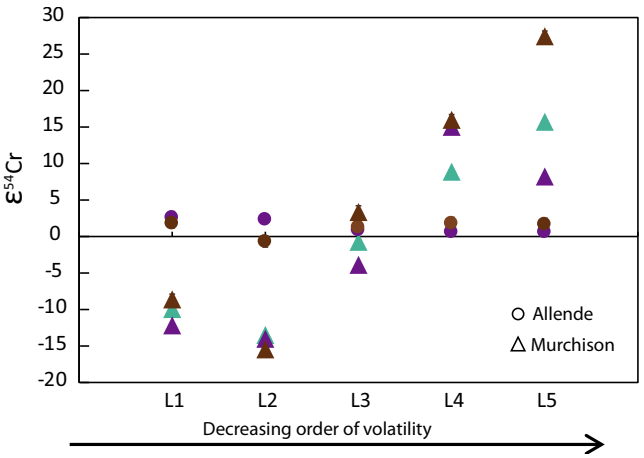

Fig. 6. $\varepsilon^{54}Cr$ variation in leachates of whole rocks of Allende and Murchison. The leachates L1 and L2 have dissolved alteration phases such as carbonates, sulfides, and magnetite whereas L3, L4, and L5 dissolved silicates and refractory oxides. Leachate data of Allende and Murchison from Rotaru et al. (1992), Trinquier et al. (2008a, 2008b), and Yamakawa and Yin (2014). Leachates of refractory phases (L4 and L5) display positive deviations in $\varepsilon^{54}Cr$; however, the extent of variation in $\varepsilon^{54}Cr$ is different in different studies. Another difference to note is that $\varepsilon^{54}Cr$-enriched carriers occur in the L4 and L5 fractions of Murchison whereas they are heterogeneously distributed in different leachate fractions of Allende.

ε^{53}Cr from –0.27 ± 0.04 to 0.49 ± 0.16). The leachate data show that ^{53}Cr- and ^{54}Cr-enriched carrier phases were sampled by the same leachate fractions (L1, L2, and L3) of Allende (Trinquier et al. 2008b). In more strongly altered chondrites such as Murchison, Tagish Lake, Orgueil, and Sutter's Mill leachates L1, L2, and L3 dissolved ^{53}Cr-enriched carrier phases and L4 and L5 dissolved ^{54}Cr-enriched carriers (Trinquier et al. 2008b; Petitat et al. 2011; Yamakawa and Yin 2014). This might reflect heterogeneous distribution of different carrier phases of ^{53}Cr and ^{54}Cr in chondrite groups or variable ingrowth of ^{53}Cr (due to ^{53}Mn decay) during the lifetime of ^{53}Mn. In physically separated components of Murchison, a clear separation of ^{53}Cr- and ^{54}Cr-rich or depleted phases is not possible on the mineral scale; however, endmember compositions of ε^{53}Cr as in leachates can be identified in slightly magnetic and magnetic fractions (Table 1). Scattered variations are observed between ε^{53}Cr and ^{55}Mn/^{52}Cr in physically separated components as well as in leachates (Fig. 3). In chondrites of petrologic types 2 and 3, ε^{53}Cr-enriched phases are present in the Mn-enriched leaching fractions (Rotaru et al. 1992; Trinquier et al. 2008b; Petitat et al. 2011; Yamakawa and Yin 2014) and such phases appear to be not dissolved in Cr-enriched fractions. Despite their variable alteration histories, the variation of ε^{53}Cr in physically separated components and leachates (Fig. 1) of Allende and Murchison are of similar magnitude. This suggests that variations in ε^{53}Cr and ^{55}Mn/^{52}Cr were not homogenized on the component scale during thermal metamorphism on the Allende meteorite parent body or aqueous alteration on the Murchison parent body.

The leachates from Murchison show tenfold higher ε^{54}Cr compared to Allende leachates. The likely cause of this isotopic difference and of the different behavior of the anomalies is the preservation of isotopically anomalous Cr carrier phases in the matrix of Murchison (Trinquier et al. 2008b). Temperatures of metamorphism of Allende were approximately 800–900 K, whereas aqueous alteration of Murchison occurred at 300–425 K (Huss and Lewis 1994). Leachate fractions of Murchison which sample carbonates, sulfides, and other matrix phases show lower ε^{54}Cr relative to bulk rocks (Trinquier et al. 2008b; Yamakawa and Yin 2014). The positive ε^{54}Cr in refractory components such as leachate fractions of Murchison and Allende CAIs likely reflect initial heterogeneity of the ^{54}Cr carrier phases. The diminishing of anomalies of ε^{54}Cr in leachates of Allende compared to Murchison leachates by thermal metamorphism of Allende is plausible. ^{54}Cr-enriched carrier phases (identified in CI chondrites), such as spinels, remained enclosed in CAIs or other coarse-grained silicates and are difficult to destroy at metamorphic conditions relevant for types 1–3 CCs. Thus, such phases preserve large ^{54}Cr anomalies (Dauphas et al. 2010; Nittler et al. 2018). However, Cr in spinel and olivine grains within the matrix and on the rims of altered fine-grained CAIs and chondrules may have been modified during thermal metamorphism, and thus, the ^{54}Cr anomalies could have been diminished by exchange with isotopically different Cr in the matrix. Therefore, the initial heterogeneity in the Cr isotope composition is mainly recorded by the highly anomalous components. Carrier phases of ^{54}Cr-depleted endmembers are likely sulfides, metals, and their alteration products.

The initial heterogeneity in ^{54}Cr can be explained by the presence of different ^{54}Cr-enriched and depleted carriers in the components of Allende and Murchison. Yamakawa and Yin (2014) proposed that at least five and possibly up to seven (EM 1-7), different ^{54}Cr- and ^{53}Cr-bearing endmembers may exist in CCs. These endmember compositions of ^{54}Cr and ^{53}Cr from Yamakawa and Yin (2014) are shown in Fig. 7 with additional literature data. In physically separated components of CC, we can identify four different ^{54}Cr and ^{53}Cr carriers (Figs. 2 and 3b). A ^{54}Cr-enriched and ^{53}Cr-depleted endmember (EM 1) is mostly residing in magnetic fractions. Endmembers, EM 2 and EM 4, represent coupled enrichments of ^{54}Cr and ^{53}Cr and occur in the chondrule fractions, matrix-rich and slightly magnetic fractions. The CAI fraction and the nonmagnetic fraction represent variable mixing of endmembers EM 1 and EM 6.

Large ^{54}Cr anomalies in the Murchison leachate fractions (Rotaru et al. 1992; Trinquier et al. 2008b; Yamakawa and Yin 2014) are homogenized in the physically separated components due to admixture of other endmembers (mostly EM 6). Additional thermal processing in the solar nebula, for instance during chondrule formation, may also have contributed to the homogenization and reduction of large anomalies. Further homogenization of ^{54}Cr-enriched and depleted carrier phases in matrix may have occurred during parent body metamorphism and small-scale redistribution processes (e.g., formation of hydrous phases). The ^{54}Cr-enriched component was added to chondrite precursors along with neutron-rich isotopes of elements such as Ti, Ni, and Zr (Birck and Lugmair 1988; Leya et al. 2009; Mercer et al. 2015). ^{54}Cr-depleted carriers were either formed before the addition of ^{54}Cr from supernova ejecta or could have resulted from submicrometer-scale heterogeneity of ^{54}Cr carrier phases in precursor dust. The nebular composition before the addition of ^{54}Cr-carriers to precursor dust would be representative of the solar ^{54}Cr abundance.

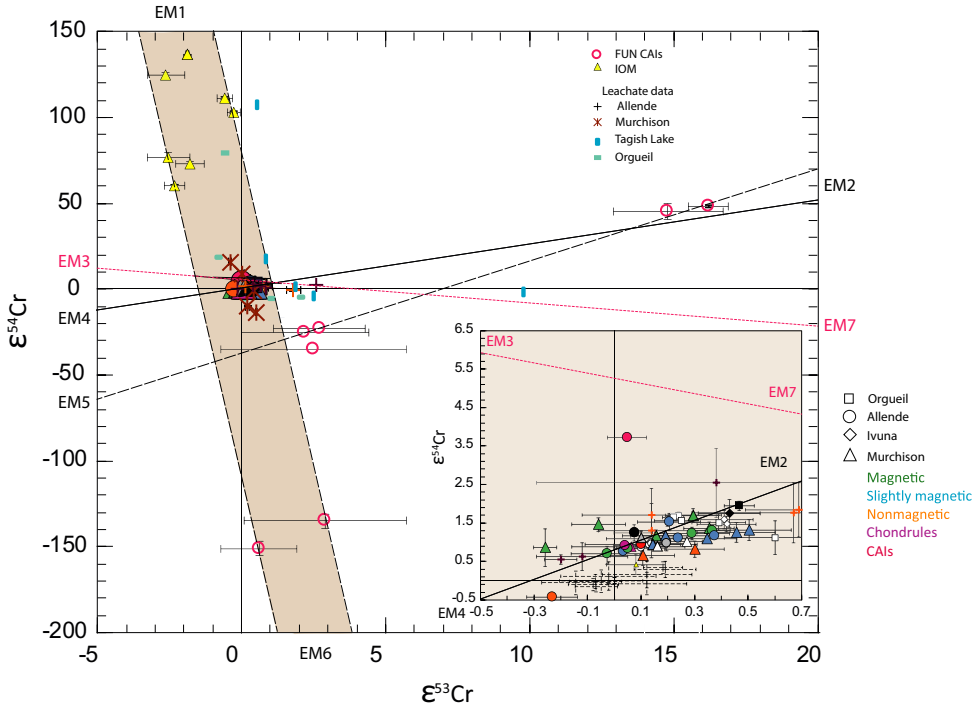

Fig. 7. $\varepsilon^{54}Cr$-$\varepsilon^{53}Cr$ data from the present study and the literature, the latter including physically separated components (mainly CAIs and chondrules), whole rock leachates, and insoluble organic matter (IOM) from Allende, Murchison, Orgueil, and Tagish Lake (Papanastassiou 1986; Birck and Allègre 1988; Birck and Lugmair 1988; Papanastassiou and Brigham 1989; Bogdanovski et al. 2002; Trinquier et al. 2008b; Qin et al. 2010; Petitat et al. 2011; Yamakawa and Yin 2014; Mercer et al. 2015). Presumed endmember compositions (EM 1, EM 2, EM 3, EM 4, EM 7) of ^{57}Cr and ^{53}Cr are from fig. 4 of Yamakawa and Yin (2014). Endmember compositions EM 6 and EM 5 from the aforementioned study were modified using FUN-CAI data (Papanastassiou and Brigham 1989). The $\varepsilon^{54}Cr$-$\varepsilon^{53}Cr$ variation of the bulk rocks of carbonaceous chondrites and physically separated components of Allende and Murchison from this study can be explained by a mixture of EM 1, EM 2, EM 3, EM 4, and EM 6 endmembers (shown by the tan field). For details, see Discussion in the main text.

The data on leachates and components analyzed so far suggest that the lowest $\varepsilon^{54}Cr$ value of the early solar system material might be as low as -151.0 ± 4.2. Further detailed study of chemical compositions and isotope variations of elements such as Ti, Ni, and Ca in ^{54}Cr-depleted carriers are required to distinguish the roles of initial heterogeneity and thermal processing in early solar system material.

Cr Isotopes and Isotopic Complementarity of Components in CV and CM Chondrites

Chemical and isotopic complementarity between matrix and chondrules of some CC groups has been noted for abundances and isotope ratios (notably $^{183}W/^{184}W$) of several elements in CCs (Bland et al. 2005; Hezel and Palme 2008, 2010; Palme et al. 2015; Budde et al. 2016a, 2016b). These studies show that the bulk compositions of these chondrites cannot represent arbitrary mixtures of matrix and chondrules with nonsolar compositions, because the bulk compositions are always solar in composition. These data imply that matrix, chondrules, and their precursors represent the products of closed-system thermal processing (e.g., chondrule formation) in localized domains of the solar nebula. Individual Allende chondrules show ~50% difference in $\varepsilon^{50}Ti$ relative to the bulk rock, which can be explained by addition of isotopically anomalous grains to the chondrule precursors (Gerber et al. 2017). Isotope ratios of Mg and Cr of individual chondrules are variable, which was interpreted to indicate that chondrules with different isotopic compositions were likely formed in different regions of the solar system and were mixed before accretion, which would rule out close genetic links between chondrules and matrix (Olsen et al. 2016). However, in the latter study, no measurements were carried out on matrix samples. Our bulk chondrule data from Allende and Murchison plot as an endmember with lower $\varepsilon^{53}Cr$, $\varepsilon^{54}Cr$, and lowest Mn/Cr ratio compared to other components and bulk rocks (Figs. 1 and 2; Table 1). Three individual Allende chondrules were analyzed previously for $\varepsilon^{54}Cr$ and show

values of –0.08 ± 0.11, –0.58 ± 0.09, and –0.36 ± 0.09, respectively (Trinquier et al. 2007; Connelly et al. 2012). The higher value of ε^{54}Cr of Allende bulk chondrules in this study suggests that the Allende chondrules with higher $^{54}Cr/^{52}Cr$ were not sampled in previous studies. Variability of ε^{53}Cr, ε^{54}Cr, and Mn/Cr also exists in fine-grained matrix-rich components (<80 μm) of both meteorites. If CCs sampled material from various regions of the solar system and chondrule and matrix formed in different regions of the solar nebula, then the similarity of calculated and analyzed bulk rock ε^{54}Cr in Allende and Murchison would be a coincidence. As it occurs for both meteorites, a coincidence appears rather improbable. Thus, we conclude that chondrules and matrix in these CCs were derived from different, but homogeneous dust–gas reservoirs, which contained isotopically heterogeneous precursors of chondrules and matrix, which on average (on a gram level of sample weight) have a similar isotopic composition as the bulk rock. The "internal isotopic differentiation" of these grains was facilitated by variable and multiple thermal processing of dust grains, with chondrules and matrix as the manifestations of the last high-temperature processing.

To conclude, an origin of chondrules and matrix of CCs in different regions of the solar nebula is not required. The variability of ε^{54}Cr and ε^{53}Cr in CCs of a particular group can be explained by initial heterogeneity and variable thermal processing of the precursor material in the same feeding zone and mixing processes. Different isotopic compositions of different chondrite groups may reflect differences in thermal processing conditions (e.g., temperature and fO_2), but heliocentric and temporal gradients in grain compositions may play a role as well.

SUMMARY AND CONCLUSIONS

High-precision chromium isotope data of bulk rocks of Allende, Orgueil, and Ivuna agree within uncertainty with previous studies, which confirm the accuracy of our sample preparation methods and analysis procedure. Correlated variations of ε^{53}Cr (also ε^{54}Cr) and $^{55}Mn/^{52}Cr$ in the bulk rocks plot on the bulk chondrite isochron from Trinquier et al. (2008b) with an age of 4567.3 ± 1.9 Myr, which indicates the homogeneity of Cr-isotope composition of 0.1–1 g aliquots of bulk rock powders of these CCs.

Physically separated components were prepared from gram-size aliquots of Allende and Murchison to obtain their $^{55}Mn/^{52}Cr$ and Cr isotopic compositions. Deviations of some components from the bulk CC isochron are plausibly explained by localized redistribution of Mn during aqueous alteration after most ^{53}Mn has decayed. Coupled low $^{55}Mn/^{52}Cr$ ratio and ε^{53}Cr in a few components such as chondrules reflects early thermal processing in the solar nebula and retarded ingrowth of ^{53}Cr. Higher $^{55}Mn/^{52}Cr$ and ε^{53}Cr in some magnetic and slightly magnetic components and matrix indicate a certain level of complementarity in chemical compositions of the Fe- and volatile-rich matrix and Fe-poor chondrules and refractory element enriched nonmagnetic material. Mass balance shows that chemical and Cr isotopic heterogeneities at the scale of different components are homogenized in the bulk rocks at the 1 g scale to yield compositions consistent with other bulk rock measurements. This observation and the complementarity of chemical and some isotopic compositions of chondrules and matrix in these meteorites (Hezel and Palme 2008, 2010; Palme et al. 2015; Budde et al. 2016a, 2016b) support the view that on a bulk scale, CV and CM chondrites and their components formed in nebular domains with a specific composition different from other domains.

At least four different endmembers, (EM 1, EM 2, EM 4, and EM 6 of Yamakawa and Yin 2014) showing nucleosynthetic variations of Cr isotopes in CV and CM meteorites are required to explain the data on physically separated components: Positive ε^{54}Cr may be coupled with negative ε^{53}Cr, or both ε^{54}Cr and ε^{53}Cr are positive. Negative ε^{54}Cr and ε^{53}Cr occur in the nonmagnetic fraction of Allende, whereas positive ε^{54}Cr also occurs with normal (terrestrial) ε^{53}Cr. The carrier phases enriched in ^{54}Cr only are mainly concentrated in the CAI fraction from Allende. The latter may reflect initial heterogeneity in both ^{53}Cr and ^{54}Cr in the early solar system, exposed by later thermal processing and alteration in the solar nebula and on the parent body. However, it is also possible that the apparent deficit in ^{53}Cr in some samples (some of them enriched in refractory elements) reflect initially low Mn/Cr and later disturbance of their Mn/Cr ratio. The discrepancy between the negative correlation of ε^{53}Cr and ε^{54}Cr observed in leachate studies (Trinquier et al. 2007; Yamakawa and Yin 2014) and more limited and scattered variations of ε^{53}Cr and ε^{54}Cr in physically separated components likely reflects the different sampling of endmembers by these methods, but also variable thermal processing of different Cr carrier phases during metamorphic heating.

Acknowledgments—We gratefully acknowledge the Field Museum, Chicago, for providing Allende and Murchison sample chips; Museum für Naturkunde, Berlin for providing Orgueil sample powder; and the Natural History Museum in Washington, D.C., for an aliquot of the Ivuna and Smithsonian Allende standard powder. We thank F. Schubring, Emil Jarosz, and M.

Feth for assistance and support in the clean chemistry laboratory. We thank Anne Trinquier for discussions regarding the analytical methods. We thank Sara Russell and Adrian Brearley for constructive reviews and comments which improved the manuscript significantly. This work was funded by DFG-SPP 1385 "The first ten million years of solar system—a planetary materials approach" (BE1820/10-1/2).

Editorial Handling—Dr. Adrian Brearley

REFERENCES

Birck J.-L. and Allègre C. J. 1985. Evidence for the presence of ^{53}Mn in the early solar system. *Geophysical Research Letters* 12:745–748.

Birck J.-L. and Allègre C. J. 1988. Manganese chromium isotope systematics and development of the early solar system. *Nature* 331:579–584.

Birck J.-L. and Lugmair G. W. 1988. Nickel and chromium isotopes in Allende inclusions. *Earth and Planetary Science Letters* 90:131–143.

Bland P. A., Alard O., Benedix G. K., Kearsley A. T., Menzies O. N., Watt L. E., and Rogers N. W. 2005. Volatile fractionation in the early solar system and chondrule/matrix complementarity. *Proceedings of the National Academy of Sciences of the United States of America* 102:13,755–13,760.

Bland P. A., Jackson M. D., Coker R. F., Cohen B. A., Webber J. B. W., Lee M. R., Duffy C. M., Chater R. J., Ardakani M. G., McPhail D. S., McComb D. W., and Benedix G. K. 2009. Why aqueous alteration in asteroids was isochemical: High porosity ≠ high permeability. *Earth and Planetary Science Letters* 28:559–568.

Bogdanovski O., Papanastasiou D.A., and Wasserburg G. J. 2002. Cr isotopes in Allende Ca-Al-rich inclusions (abstract #1802). 33rd Lunar and Planetary Conference. CD-ROM.

Brearley A. J. and Krot A. N. 2013. Metasomatism in the early solar system: The record from chondritic meteorites. In *Metasomatism and the chemical transformation of rock*. Lecture Notes in Earth System Sciences. Berlin: Springer. pp. 653–782.

Brearley A. J., Fagan T. J., Washio M., and MacPherson G. J. 2014. FIB-TEM characterization of dmisteinbergite with intergrown biopyriboles in Allende Ca-Al-rich inclusions: Evidence for alteration in the presence of aqueous fluid (abstract #2287). 45th Lunar and Planetary Science Conference. CD-ROM.

Budde G., Burkhardt C., Brennecka G. A., Fischer-Gödde M., Kruijer T. S., and Kleine T. 2016a. Molybdenum isotopic evidence for the origin of chondrules and a distinct genetic heritage of carbonaceous and non-carbonaceous meteorites. *Earth and Planetary Science Letters* 454:293–303.

Budde G., Kleine T., Kruijer T. S., Burkhardt C., and Metzler K. 2016b. Tungsten isotopic constraints. *Proceedings of the National Academy of Sciences of the United States of America*. 113:2886–2891.

Burkhardt C., Kleine T., Dauphas N., and Wieler R. 2012. Nucleosynthetic tungsten isotope anomalies in acid leachates of the Murchison chondrite: Implications for hafnium-tungsten chronometry. *Astrophysical Journal Letters* 753:L1–L6.

Clayton D. D. 2003. *Handbook of isotopes in the cosmos: Hydrogen to gallium*. Cambridge: Cambridge University Press.

Connelly J. N., Bizzarro M., Krot A. N., Nordlund A., Wielandt D., and Ivanova M. A. 2012. The absolute chronology and thermal processing of solids in the solar protoplanetary disk. *Science* 338:651–655.

Dauphas N., Marty B., and Reisberg L. 2002. Molybdenum nucleosynthetic dichotomy revealed in primitive meteorites. *The Astrophysical Journal Letters* 569:L139–L142.

Dauphas N., Remusat L., Chen J. H., Roskosz M., Papanastassiou D. A., Stodolna J., Guan Y., and Ma C. 2010. Neutron-rich chromium isotope anomalies in supernova nanoparticles. *Astrophysical Journal* 720:1577–1591.

Davis A. M., Simon S. B., and Grossman L. 1994. Alteration of Allende Type B1 CAIs: When, where, and how? 25th Lunar and Planetary Science Conference. p. 315.

Fischer-Gödde M., Burkhardt C., Kruijer T. S., and Kleine T. 2015. Ru isotope heterogeneity in the solar protoplanetary disk. *Geochimica et Cosmochimica Acta* 168:151–171.

Fujiya W., Sugiura N., and Sano Y. 2011. Mn-Cr age of dolomite in the Ivuna CI chondrite (abstract #1397). 42nd Lunar and Planetary Conference. CD-ROM.

Fujiya W., Sugiura N., Hotta H., Ichimura K., and Sano Y. 2012. Evidence for the late formation of hydrous asteroids from young meteoritic carbonates. *Nature Communications* 3:1–6.

Gerber S., Burkhardt C., Budde G., Metzler K., and Kleine T. 2017. Mixing and transport of dust in the early solar nebula as inferred from titanium isotope variations among chondrules. *The Astrophysical Journal Letters* 84:1–7.

Grossman J. N. and Brearley A. J. 2005. The onset of metamorphism in ordinary and carbonaceous chondrites. *Meteoritics & Planetary Science* 40:87–122.

Hartmann P. S., Woosley E., and El Eid M. F. 1985. Nucleosynthesis in neutron-rich supernovae ejecta. *The Astrophysical Journal* 297:837–845.

Hezel D. C. and Palme H. 2008. Constraints for chondrule formation from Ca–Al distribution in carbonaceous chondrites. *Earth and Planetary Science Letters* 265:716–725.

Hezel D. C. and Palme H. 2010. The chemical relationship between chondrules and matrix and the chondrule matrix complementarity. *Earth and Planetary Science Letters* 294:85–93.

Hidaka H., Ohta Y., and Yoneda S. 2003. Nucleosynthetic components of the early solar system inferred from Ba isotopic compositions in carbonaceous chondrites. *Earth and Planetary Science Letters* 214:455–466.

Honda M. and Imamura M. 1971. Half-life of ^{53}Mn. *Physical Review C* 4:1182–1188.

Huss G. R. and Lewis R. S. 1994. Noble gases in presolar diamonds II: Component abundances reflect thermal processing. *Meteoritics* 29:811–829.

Johnson C. A. and Prinz M. 1993. Carbonate compositions in CM and CI chondrites, and implications for aqueous alteration. *Geochimica et Cosmochimica Acta* 57:2843–2852.

Kadlag Y. and Becker H. 2016. Highly siderophile and chalcogen element constraints on the origin of components of the Allende and Murchison meteorites. *Meteoritics & Planetary Science* 51:1136–1152.

Kallemeyn G. W. and Wasson J. T. 1981. The compositional classification of chondrites I: the carbonaceous chondrite groups. *Geochimica et Cosmochimica Acta* 45:1217–1230.

Krot A. N., Scott E. R. D., and Zolensky M. E. 1995. Mineralogical and chemical modification of components in CV3 chondrites: Nebular or asteroidal processing? *Meteoritics* 30:748–775.

Leya I., Schönbächler M., Krähenbühl U., and Halliday A. N. 2009. New titanium isotope data for Allende and Efremovka CAIs. *The Astrophysical Journal* 702:1118–1126.

Lodders K. 2003. Solar system abundances and condensation temperatures of the elements. *The Astrophysical Journal* 591:1220–1247.

Lugmair G. W. and Shukolukov A. 1998. Early solar system timescales according to ^{53}Mn-^{53}Cr systematics. *Geochimica et Cosmochimica Acta* 16:2863–2886.

Mercer C. M., Souders A. K., Romaniello S. J., Williams C. D., Brennecka G. A., and Wadhwa M. 2015. Chromium and titanium isotope systematics of Allende CAIs (abstract #2920). 46th Lunar and Planetary Science Conference. CD-ROM.

Moynier F., Yin Q.-Z., and Jacobsen B. 2007. Dating the first stage of planet formation. *The Astrophysical Journal* 671: L181–L183.

Niemeyer S. 1988. Titanium isotopic anomalies in chondrules from carbonaceous chondrites. *Geochimica et Cosmochimica Acta* 52:309–318.

Nittler L. R., Alexander C. M. O'D., Liu N., and Wang J. 2018. Extremely ^{54}Cr-and ^{50}Ti-rich presolar oxide grains in a primitive meteorite: Formation in rare types of supernovae and implications for the astrophysical context of the solar system birth. *The Astrophysical Journal Letters* 856:L1–L24.

Norman E. B. 1985. Improved limits on the double beta decay half-lives of ^{50}Cr, ^{64}Zn, ^{92}Mo, and ^{96}Ru. *Physical Review C* 31:1937–1940.

Nyquist L., Lindstrom D., Shih C.-Y., Wiesmann H., Mittlefehldt D., Wentworth S., and Martinez R. 2001. Mn–Cr formation intervals for chondrules from the Bishunpur and Chainpur meteorites. *Meteoritics & Planetary Science* 36:911–938.

Nyquist L. E., Kleine T., Shih C.-Y., and Reese Y. D. 2009. The distribution of short-lived radioisotopes in the early solar system and the chronology of asteroid accretion, differentiation, and secondary mineralization. *Geochimica et Cosmochimica Acta* 73:5115–5136.

Olsen M. B., Wielandt D., Schiller M., Elishevah M. M. E., Kooten V., and Bizzarro M. 2016. Magnesium and ^{54}Cr isotope compositions of carbonaceous chondrite chondrules-Insights into early disk processes. *Geochimica et Cosmochimica Acta* 191:118–138.

Palme H., Hezel D. C., and Ebel D. S. 2015. The origin of chondrules: Constraints from matrix composition and matrix-chondrule complementarity. *Earth and Planetary Science Letters* 411:11–19.

Papanastassiou D. A. 1986. Chromium isotopic anomalies in the Allende meteorite. *The Astrophysical Journal Letters* 308:L27–L30.

Papanastassiou D. A. and Brigham C. A. 1989. The identification of meteorite inclusions with isotope anomalies. *The Astrophysical Journal Letters* 338: L37–L40.

Petitat M., Birck J.-L., Luu T. H., and Gounelle M. 2011. The chromium isotopic composition of the ungrouped carbonaceous chondrite Tagish Lake. *The Astrophysical Journal* 736:1–8.

Posner E. S., Ganguly J., and Hervig R. 2016. Diffusion kinetics of Cr in spinel: Experimental studies and implications for ^{53}Mn-^{53}Cr cosmochronology. *Geochimica et Cosmochimica Acta* 174:20–35.

Qin L., Alexander C. M. O'D., Nittler L. R., Wang J., and Carlson R. W. 2009. Looking for the carrier phase of ^{54}Cr in the carbonaceous chondrite Orgueil (abstract# 5286). *Meteoritics & Planetary Science* 72:A171.

Qin L., Alexander C. M. O'D., Carlson R. W., Horan M. F., and Yokoyama T. 2010. Contributors to chromium isotope variation of meteorites. *Geochimica et Cosmochimica Acta* 74:1122–1145.

Qin L., Nittler L. R., Alexander C. M. O'D., Wang J., Stadermann F. J., and Carlson R. W. 2011. Extreme ^{54}Cr-rich nano-oxides in the CI chondrite Orgueil-Implication for a late supernova injection into the solar system. *Geochimica et Cosmochimica Acta* 75:629–644.

Reisberg L., Dauphas N., Luguet A., Pearson D. G., Gallino R., and Zimmermann C. 2009. Nucleosynthetic osmium isotope anomalies in acid leachates of the Murchison meteorite. *Earth and Planetary Science Letters* 277:334–344.

Riciputi L. R., McSween H. Y. Jr, Johnson C. A., and Martin P. 1994. Minor and trace element concentrations in carbonates of carbonaceous chondrites, and implications for the compositions of coexisting fluids. *Geochimica et Cosmochimica Acta* 58:1343–1351.

Rotaru M., Birck J.-L., and Allègre C. J. 1990. Chromium isotopes in C chondrites: isotopic heterogeneity and further evidence for extinct ^{53}Mn. 19th Lunar and Planetary Science Conference. p. 1037.

Rotaru M., Birck J.-L., and Allègre C. J. 1992. Clues to early Solar System history from chromium isotopes in carbonaceous chondrites. *Nature* 358:465–470.

Schiller M., Paton C., and Bizzarro M. 2015. Evidence for nucleosynthetic enrichment of the protosolar molecular cloud core by multiple supernova events. *Geochimica et Cosmochimica Acta* 149:88–102.

Schiller M., Bizzarro M., and Fernandes V. A. 2018. Isotopic evolution of the protoplanetary disk and the building blocks of Earth and the Moon. *Nature* 555:507–510.

Schultz L. and Franke L. 2004. Helium, neon, and argon in meteorites: A data collection. *Meteoritics & Planetary Science* 39:1889–1890.

Schönbächler M., Lee D.-C., Rehkämper M., Halliday A. N., Fehr M. A., Hattendorf B., and Günther D. 2003. Zirconium isotope evidence for incomplete admixing of r-process components in the solar nebula. *Earth and Planetary Science Letters* 216:467–481.

Schönbächler M., Rehkämper M., Fehr M. A., Halliday A. N., Hattendorf B., and Günther D. 2005. Nucleosynthetic zirconium isotope anomalies in acid leachates of carbonaceous chondrites. *Geochimica et Cosmochimica Acta* 69:5113–5122.

Shields W. R., Murphy J. T., Cantazaro E. J., and Garner E. L. 1966. Absolute isotopic abundance ratios and the atomic weight of a reference sample of chromium. *Journal of Research of the National Bureau of Standards* 70A:193–197.

Shima W. and Honda M. 1966. Distribution of spallation produced chromium between alloys in iron meteorites. *Earth and Planetary Science Letters* 1:65–74.

Shukolyukov A. and Lugmair G. W. 2004. Manganese–chromium isotope systematics of enstatite meteorites. *Geochimica et Cosmochimica Acta* 68:2875–2888.

Shukolyukov A. and Lugmair G. W. 2006. Manganese–chromium isotope systematics of carbonaceous chondrites. *Earth and Planetary Science Letters* 250:200–213.

Trinquier A., Birck J.-L., and Allègre C. J. 2007. Widespread ^{54}Cr heterogeneity in the inner solar system. *Astrophysical Journal* 655:1179–1185.

Trinquier A., Birck J.-L., and Allègre C. J. 2008a. High-precision analysis of chromium isotopes in terrestrial and meteorite samples by thermal ionization mass spectrometry. *Journal of Analytical Atomic Spectrometry* 23:1565–1574.

Trinquier A., Birck J.-L., Allègre C. J., Göpel C., and Ulfbeck D. 2008b. ^{53}Mn–^{53}Cr systematics of the early Solar System revisited. *Geochimica et Cosmochimica Acta* 72:5146–5163.

Trinquier A., Elliott T., Ulfbeck D., Coath C., Krot A. N., and Bizzarro M. 2009. Origin of nucleosynthetic isotope heterogeneity in the solar protoplanetary disk. *Science* 324:374–376.

Wang Z., Becker H., and Wombacher F. 2015. Mass fractions of S, Cu, Se, Mo, Ag, Cd, In, Te, Ba, Sm, W, TI and Bi in geological reference materials and selected carbonaceous chondrites determined by isotope dilution ICP-MS. *Geostandards and Geoanalytical Research* 39:185–208.

Woosley S. E., Heger A., and Waever T. A. 2002. The evolution and explosion of massive stars. *Reviews of Modern Physics* 74:1015–1071.

Yamakawa A. and Yin Q.-Z. 2014. Chromium isotopic systematics of the Sutter's Mill carbonaceous chondrite: Implications for isotopic heterogeneities of the early solar system. *Meteoritics & Planetary Science* 49:2118–2127.

Yamashita K., Maruyama S., Yamakawa A., and Nakamura E. 2010. ^{53}Mn-^{53}Cr chronometry of CB chondrite: Evidence for uniform distribution of ^{53}Mn in the early solar system. *The Astrophysical Journal* 723:20–24.

Yokoyama T., Rai V. K., Alexander C. M. O'D., Lewis R. S., Carlson R. W., Shirey S. B., Thiemens M. H., and Walker R. J. 2007. Osmium isotope evidence for uniform distribution of s- and r- process components in the early solar system. *Earth and Planetary Science Letters* 259:567–580.

Zinner E., Nittler L. R., Hoppe P., Gallino R., Straniero O., and Alexander C. M. O'D. 2005. Oxygen, magnesium and chromium isotopic ratios of presolar spinel grains. *Geochimica et Cosmochimica Acta* 69:4149–4165.

SUPPORTING INFORMATION

Additional supporting information may be found in the online version of this article.

Fig. S1. Optical microscope photographs of physically and magnetically separated components of the Allende meteorite. Scale bar on images is 1000 μm, except for the matrix fraction, which is 100 μm. In case of chondrules and CAIs, only particles without matrix attached were digested.

Fig. S2. Optical microscope photographs of physically and magnetically separated components of the Murchison meteorite. Scale bar on all images is 1000 μm.